Combustion and Flame 157 (2010) 155–166

Contents lists available at ScienceDirect

Combustion and Flame

journal homepage: www.elsevier.com/locate/combustflame

Time- and space-resolved quantitative LIF measurements of formaldehyde in a heavy-duty diesel engine

A.J. Donkerbroek [a], A.P. van Vliet [a], L.M.T. Somers [b], P.J.M. Frijters [b], R.J.H. Klein-Douwel [a], N.J. Dam [a,b,*], W.L. Meerts [a], J.J. ter Meulen [a]

[a] Institute for Molecules and Materials, Applied Physics, Radboud University Nijmegen, Toernooiveld 1, 6525 ED Nijmegen, The Netherlands
[b] Mechanical Engineering, Eindhoven University of Technology, P.O. Box 513, 5600 MB Eindhoven, The Netherlands

ARTICLE INFO

Article history:
Received 30 March 2009
Received in revised form 20 May 2009
Accepted 6 July 2009
Available online 13 August 2009

Keywords:
Formaldehyde
Diesel engine
Quantitative
LIF

ABSTRACT

Formaldehyde (CH_2O) is a characteristic species for the ignition phase of diesel-like fuels. As such, the spatio-temporal distribution of formaldehyde is an informative parameter in the study of the ignition event in internal combustion engines, especially for new combustion modes like homogeneous charge compression ignition (HCCI). This paper presents quantitative data on the CH_2O distribution around diesel and *n*-heptane fuel sprays in the combustion chamber of a commercial heavy-duty diesel engine. Excitation of the 4_0^1 band (355 nm) as well as the $4_0^1 2_0^1$ band (339 nm) is applied. We use quantitative, spectrally resolved laser-induced fluorescence, calibrated by means of formalin seeding, to distinguish the contribution from CH_2O to the signal from those of other species formed early in the combustion. Typically, between 40% and 100% of the fluorescence in the wavelength range considered characteristic for formaldehyde is in fact due to other species, but the latter are also related to the early combustion. Numerical simulation of a homogeneous reactor of *n*-heptane and air yields concentrations that are in reasonable agreement with the measurements. Formaldehyde starts to be formed at about 2 °CA (crank angle degrees) before the rise in main heat release. There appears to be a rather localised CH_2O formation zone relatively close to the injector, out of which formaldehyde is transported downstream by the fuel jet. Once the hot combustion sets in, formaldehyde quickly disappears.

1. Introduction

The current dominance of heavy-duty diesel engines in powering road freight transport is unlikely to be challenged in the foreseeable future [1]. Nevertheless, legislation confronts engine manufacturers with increasingly stringent emission limits. These, of course, can be met by exhaust gas aftertreatment, but there is a fuel penalty attached. Several novel combustion concepts are under study, that hopefully maintain efficiency while reducing emissions. Ignition is a key event in the whole cycle, and ignition control is, for instance, of prime importance for combustion modes like Homogeneous (or Premixed, PCCI) Charge Compression Ignition (HCCI), in which the ignition is decoupled from the fuel injection.

Here, we focus on the formation and destruction of formaldehyde (CH_2O), a relatively stable intermediate species that occurs in appreciable amounts only during roughly the first 10% of the heat release in a typical diesel combustion cycle [2]. Its main interest lies in the fact that it indicates the first combustion stage of two-stage ignition fuels, and as such it characterises the temporal and local combustion process within the cylinder. It indicates the start of the combustion and its presence late in the expansion stroke reflects locally fuel lean areas that have not transitioned to the second stage of combustion.

Formaldehyde has been studied extensively in internal combustion engines under HCCI operation [3–6]. In relation with high-temperature combustion diesel engine studies, it has been investigated in a (surrogate) diesel spray in a rapid compression machine [7] and a high pressure vessel [8]. For late-injection low-temperature combustion, Genzale et al. [9] have used formaldehyde fluorescence to study piston bowl geometry effects on the combustion process.

Quantification of CH_2O fluorescence is complicated, especially at engine conditions [3,10]. In virtually all publications dealing with two-dimensional fluorescence images (induced by the 3rd harmonic of a Nd:YAG laser), spectral filters are used to single out wavelength bands that are considered to be characteristic for CH_2O fluorescence. The spatially resolved light that is detected is then interpreted as originating (partly) from formaldehyde, an assumption not always carefully justified. The large variety of heavy intermediate species (which possibly fluoresce in a wide wavelength range) that occurs during the start of combustion, however, necessitates a careful interpretation of 2D fluorescence images.

* Corresponding author. Address: Institute for Molecules and Materials, Applied Physics, Radboud University Nijmegen, Toernooiveld 1, 6525 ED Nijmegen, The Netherlands. Fax: +31 243653311.
E-mail address: n.dam@science.ru.nl (N.J. Dam).

0010-2180/$ - see front matter © 2009 The Combustion Institute. Published by Elsevier Inc. All rights reserved.
doi:10.1016/j.combustflame.2009.07.004

Table 1
Specifications and global operating conditions of the measurement cylinder.

Engine type	Six-cylinder four-stroke DI diesel engine
Bore, stroke	130 mm, 146 mm
Displacement	1.939 l (per cylinder)
Compression ratio	15 (unmodified: 16)
Piston bowl shape	"Bath tub" (flat piston window)
∅ Piston bowl	84 mm
Swirl number	1.8
∅ Injector, # holes	0.128 mm, 8
Amount of diesel injected, inj. pressure	60 mg of low-sulphur diesel, 120 MPa (eight holes opened)
Injection duration, diesel	17.5 °CA
Amount of *n*-heptane injected, inj. pressure	48 ± 5 mg of *n*-heptane, 85 MPa (eight holes opened)
Injection duration, *n*-heptane	17.0 °CA
Nominal boost pressure	0.12 and 0.14 MPa (abs.; no EGR)
Engine speed	1430 rpm
Distance injector tip to cylinder head	1.9 mm

We here report quantitative measurements on formaldehyde within the combustion chamber of an optically-accessible diesel engine by laser-induced fluorescence (LIF) as a function of time and position, employing a range of injection timings. It has been systematically investigated what part (if any) of the total fluorescence is due to CH_2O. The main focus is on the (unsteady) premixed combustion phase. Two laser sources have been used, the 3rd harmonic of an Nd:YAG laser and a tunable dye laser, probing the 4_0^1 or the $4_0^1 2_0^1$ vibrational band of the $\widetilde{A}^1A_2 \leftarrow \widetilde{X}^1A_1$ electronic transition, respectively.

The fuels used are commercial low-sulphur diesel and *n*-heptane. We show that, for both fuels, the detection of fluorescence in the wavelength range of formaldehyde emission does not necessarily imply the actual presence of formaldehyde. As a consequence, 2D images will be much harder to interpret. Furthermore, we report a novel way to derive formaldehyde concentrations from fluorescence spectra recorded in a diesel spray, based on a study of the formaldehyde spectrum as a function of pressure and temperature.

2. Experiment

2.1. Engine

In Table 1, the specifications of the optical six-cylinder heavy-duty diesel engine are listed, and Fig. 1 shows the optically accessible measurement cylinder. Fuel injection into the measurement cylinder is achieved by a home-built common-rail (CR) system, providing the possibility to start and end the injection at will. The injector can be rotated around its axis, allowing measurements at different positions relative to the fuel spray without repositioning the laser beam. To avoid overheating, the non-lubricated measurement cylinder is skip-fired. With respect to temperature, steady-state conditions are mimicked by (pre-)heating the cooling water to operational temperatures.

Measurements were performed on two sprays as indicated by 1 and 2 in Fig. 1c. For measurements on spray 2, the injector hole of spray 1 was blocked to prevent excessive attenuation later in the stroke.

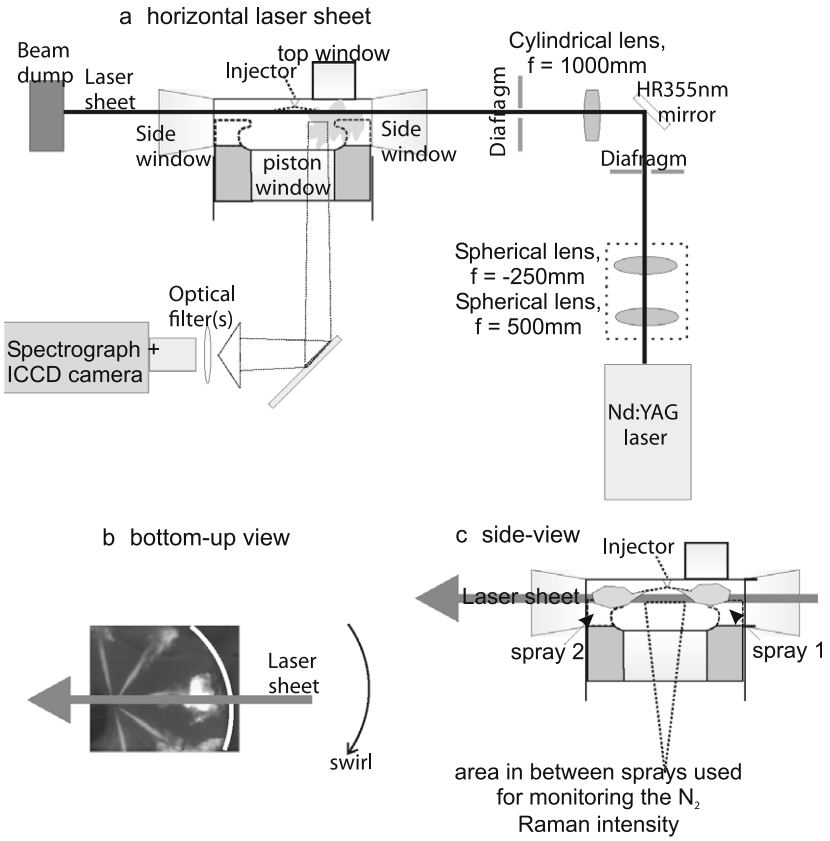

Fig. 1. Schematic representation of the setup: (a) Schematic view using the 355 nm laser sheet. In case of dye laser measurements, the two spherical lenses were replaced by an $f = 1500$ mm spherical lens and the HR355 mirror by a prism. (b) Bottom-up view of the sprays along with the position of the laser sheet. (c) Side-view of the two sprays traversed by the laser sheet.

For diesel, the start of fuel delivery (SoD), i.e. the *effective* start of injection was determined from high-speed imaging (see Fig. S1 in [11] for a more detailed description). For *n*-heptane as a fuel, no high-speed images were available. The SoD was retrieved from the rail-pressure trace and the (uncalibrated) needle-lift. In both cases the SoD occurs about 3.5° after triggering the injection system.

The start of combustion was retrieved from the rate of heat release [12], derived from the in-cylinder pressure trace. An example of typical pressure traces for both fuels, along with the rate of heat release, is depicted in Fig. 2. Diesel fuel was injected at 120 MPa. For *n*-heptane, the CR system could not reach pressures beyond 90 MPa due to the low fuel viscosity.

Two opposite slots (12 mm high and 9.5 mm wide) machined in the piston crown allow observations and laser access through both side windows even at top dead centre (TDC). The slots do not significantly affect the overall combustion characteristics. High-speed images of the combustion luminosity (mainly soot) [11] show that the development of combustion is similar for all sprays. Separate results (not shown here; paper in preparation) show that also the OH chemiluminescence behaves similar for all sprays, but that the flame lift-off length is slightly longer for the spray directed towards the slot than for other sprays, possibly due to reduced squish flow.

2.2. Calibration

Formalin, containing 37% formaldehyde by weight, was seeded in two ways. Firstly, it was seeded directly into the cylinder, using a direct injection petrol injector, pressurised by 3 MPa of nitrogen. The injection timing was set carefully to ensure a homogeneous distribution of formaldehyde (extracted from 2D LIF images recorded through the piston window). Alternatively, it was seeded into the inlet air, just before the inlet valves, by use of the same injector. Employing this seeding method, fluorescence measurements were performed over an extended period of time to ensure steady-state seeding. A typical seeding concentration was 0.1%. Fluorescence spectra of formaldehyde at different ambient pressures (p) and temperatures (T) were recorded by exciting the seeded formaldehyde at a range of crank angles in the motored engine. To some extent, the pressure was varied independently of the temperature by adjusting the inlet air pressure. Within experimental accuracy, both seeding methods yield similar results for the calibration factor.

2.3. CH_2O LIF measurements

Measurements were performed with an excitation laser sheet of about 1 mm thick and a width that was varied between 2 and 8 mm. The laser sheet traverses the combustion chamber parallel to the cylinder head. It typically did not propagate parallel to the spray axis, as indicated in Fig. 1c, because the sprays angle downward under 10° with the horizontal. Fluorescence was detected through the piston window. LIF of CH_2O is induced by either of two laser sources. The 3rd harmonic of a seeded Nd:YAG laser (Continuum Powerlite Precision II 8010, pulses of 40–70 mJ upon entering the cylinder) probes the 4_0^1 vibrational band of the $\widetilde{A}^1A_2 \leftarrow \widetilde{X}^1A_1$ electronic transition at 354.82 nm. A frequency-doubled dye laser (radiant dye) was used to excite the $4_0^1 2_0^1$ band at 339.017 nm. The typical pulse energy prior to entering the engine was between 1 and 3.5 mJ. The wavelength of the dye laser was calibrated by performing an excitation scan in a bunsen burner and comparing the spectrum with the CH_2O spectrum simulated by PGOPHER [13]. In the simulation, the refined spectroscopic parameters as determined by Smith et al. [14] were used. For the 3rd harmonic of the Nd:YAG laser, a linearity check of the formaldehyde fluorescence signal versus laser intensity was performed and saturation was avoided.

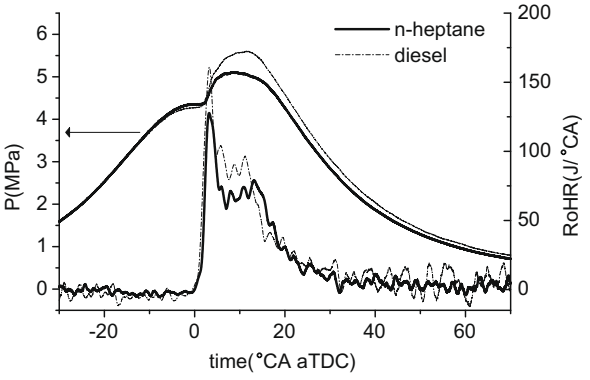

Fig. 2. Typical pressure curves and the rate of heat release (RoHR) derived from it. All eight injector holes were opened. *n*-Heptane injection between −4.5° and 12.5° after TDC (aTDC), indicated mean effective pressure (IMEP) of 438 kPa. Diesel injection between −4.5° and 10.0° aTDC, IMEP of 528 kPa.

Fluorescence spectra were recorded through the piston window, between 410 and 450 nm, using an intensified CCD camera (Roper Scientific, ICCD 512 T, 512^2 pixels, 16 bits) mounted behind a spectrograph (ARC SpectraPro 500i, 600 lines/mm grating). This wavelength range was chosen for signal strength and separation from the laser wavelength, the latter to prevent possible interference from stray light. An additional Schott GG375 filter was used in front of the collection optics to block 355 nm laser light. The entrance slit of the spectrograph was parallel to the laser sheet direction, and was opened just enough to encompass the entire width of the laser sheet for maximum intensity. Although recording the entire width of the laser sheet is accompanied by a loss of spectral resolution, Fig. 3a and b shows that the characteristic CH_2O structure (the four vibrational peaks) is still preserved. In the spectra shown, the camera images are integrated along the propagation direction of the laser. The limited repetition rate of the measurement system (10 Hz for the laser, less for the camera's) allowed only one frame to be recorded per injection event. The data in this paper are averaged over five laser shots, unless stated otherwise.

Two dimensional (that is, spectrally unresolved) measurements were performed by using the CCD camera without the spectrograph mounted. Apart from the GG375 filter, an additional SPF450 filter (CVI, transmitting between 385 and 440 nm, 63% maximum transmission) was used to block soot luminescence.

2.4. CH_2O data processing

Five pixels along the laser propagation direction were added in hardware ('binning'), before being read out by the computer, to improve the signal to noise ratio. This reduced the spatial resolution to 0.8 mm/pixel. A typical image is shown in Fig. 3c. The spectra indicated in Fig. 3 have been obtained by integrating in software the fluorescence along the laser direction (vertically in Fig. 3c).

In processing the spectra, the wavelength-dependent camera sensitivity and the transmission of the optical filter and spectrograph were taken into account by calibration with a halogen and deuterium calibration lamp with a known spectral emissivity.

3. Method of simulation

The fluorescence from formaldehyde formed in the cool flame of the premixed combustion has been quantified and this experimental concentration has been compared to simulations. It was chosen to describe this partially-premixed combustion phase by an ensemble of homogeneous reactors with varying initial conditions of *n*-heptane and air mixtures. A versatile multi-zone HCCI code is used to compute the ignition process [15]. The CH_2O concentra-

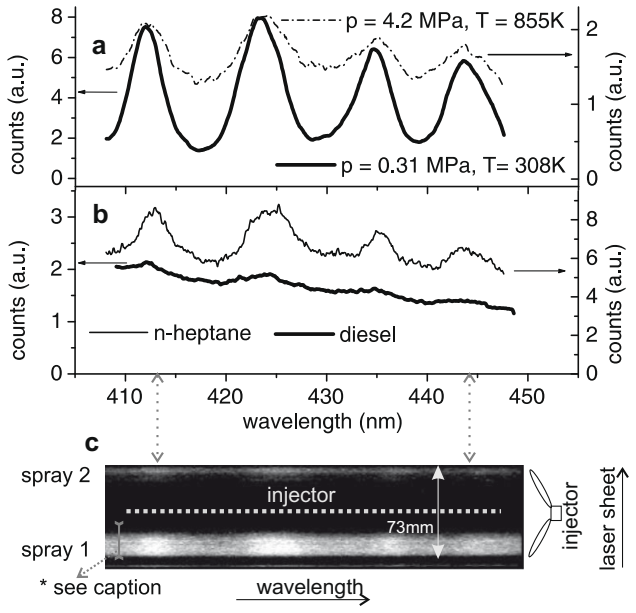

Fig. 3. (a) Two fluorescence spectra at 355 nm excitation wavelength measured in the motored engine at different pressures and temperatures. The spectra were aqcuired by seeding formalin into the inlet air of the motored engine. Note that the peaks are much less pronounced at elevated temperature and pressure. (b) Characteristic fluorescence spectrum of the firing engine fuelled with low-sulphur diesel and *n*-heptane. (c) A spatially resolved image for *n*-heptane. The dotted line represents the injector position. The wavelength scale is the same as in (a and b). In fact, it is a convolution of spatial and spectral information [36]. The vertical axis corresponds to the height of the spectrograph entrance slit, and represents spatial information only. *The region of 35 strips (strip: row of pixels) subdivided into seven parts of five strips for analysis.

tions and ignition delays provided by two reaction mechanisms have been compared to obtain information on the sensitivity of the results to the applied mechanism. The first one was the extensive LLNL PRF mechanism [16], the second a skeleton mechanism for *n*-heptane [17] (hereafter referred to as "Peters mechanism"). Because of its size, the last one is better suited to perform an extensive set of simulations.

Simulations have been performed for a wide range of equivalence ratios and initial temperatures. The mixture temperature and equivalence ratio are coupled via the temperature of the in-cylinder air (855 ± 20 K, see Appendix A) and the fuel temperature (343 ± 10 K). By performing adiabatic mixing calculations, it was analysed how the mixture temperature depends on ϕ. This temperature decreases with increasing ϕ as more fuel has to be heated up.

4. Analysis of spectra

Typical CH_2O spectra, recorded in the engine under normal operating conditions ("engine spectra") are plotted in Fig. 3, along with two spectra of CH_2O seeded into a motored engine ("seeded spectra"). The 3rd harmonic of the Nd:YAG laser was used as source of excitation. In the engine spectra, a large background accompanies four distinct characteristic peaks. The spectrum is expected to consist of three components: spectral structure due to CH_2O, a broad featureless background due to CH_2O and a broad background originating from other species (e.g. other aldehydes, fuel and PAH fluorescence). Since our aim is to quantify the CH_2O signal, the contribution of CH_2O to the whole spectrum has to be quantified.

To assess which part of the engine spectrum can be ascribed to CH_2O, we need to consider both the spectral structure and the structureless background. Lachaux and Musculus [18] introduced a method to deal with this issue, based on the covariance of Fourier-transformed sample and reference spectra. This method was later modified by Genzale et al. [9] to remove the undesired contribution of the structureless background. Below, we describe an alternative method that deals with the spectra directly. We prefer our method over that of Musculus and coworkers [9,18] because of the following three reasons. Because our method correlates raw spectra rather than (parts of their) Fourier transforms, (i) the correlation coefficients we find are a direct, quantitative measure for the contribution of CH_2O to each sample spectrum. Moreover, (ii) by Fourier transforming, the absolute spectral positions are lost and only information on repetitive structure is retained. The absolute spectral position, however, is essential for the assignment of spectral structure to chemical species. Finally (iii), we use a clean CH_2O spectrum (obtained from CH_2O vapour) as reference, rather than an engine spectrum that itself may already contain multiple contributions.

We retrieve both spectral structure and structureless background by comparison with a library of seeded spectra that were recorded separately, under similar conditions (p,T) as the engine spectra, but in the motored engine. Basically, the idea is that the relative contribution of spectral structure and structureless background may depend on pressure and temperature, but that their ratio is unlikely to depend on the chemical environment. This ratio is governed by the widths and relative strengths of the (vibronic) emission bands. The width of the observed emission bands is determined by the rotational Boltzmann envelope, because of fast thermal equilibration of the rotational distribution [19]. Also the relative strength of the emission bands is not expected to depend very much on the details of the chemical environment because of fast vibrational relaxation [20]. Indeed, it was observed that the ratio of the spectral structure and structureless background did not depend on whether formaldehyde was seeded in dry air or in pure nitrogen. Thus, this ratio can be determined from the seeded spectra (for which formaldehyde is the only contributor), and subsequently be used for the analysis of the engine spectra.

To isolate the spectral structure, a linear least-squares fit is made through each spectrum individually and subtracted from it. The results for the engine spectrum (diesel fuel) and the seeded spectrum shown in Fig. 3 are depicted in Fig. 4; we will refer to these by "CH_2O structure". Subsequently, both CH_2O structures are normalised (by $\left(\sum p_i^2\right)^{1/2}$; p_i are the pixel values) and then the engine spectrum is scaled to the seeded spectrum by χ^2-minimisation. The value of the scaling factor α ($\alpha \leqslant 1$ by definition) is interpreted as that part of the structure in the engine spectrum that can be ascribed to CH_2O. Of course, this procedure always produces a value for α, even for engine spectra in which hardly any spectral structure is observable at all. There is, however, a clear correlation between the value of the scaling parameter, α, and the intensity of the CH_2O structure, as can be seen in Fig. 5. Large values of α invariably correspond to large intensities of the CH_2O structure. This correlation can be used to determine a threshold value α_{thr} for the scaling factor α. For $\alpha > \alpha_{thr}$ we assume the unequivocal presence of a CH_2O contribution to the measured spectrum. This threshold value for α has been determined by taking the trend line through points in the region of high fit parameters values, which intersects the average spectral structure intensity for low values of α. We use $\alpha_{thr} = 0.5$.

When $\alpha < \alpha_{thr}$ we consider the structureless background not to contain a formaldehyde contribution. For those spectra for which $\alpha > \alpha_{thr}$, the contribution of CH_2O fluorescence to the background was determined. Again, the library of seeded spectra was used, which consist of structure and background from CH_2O only. From each seeded spectrum (at a given combination of (p,T)) two quantities were extracted: the total fluorescence intensity, I, and the intensity of the spectral structure, S. The total CH_2O fluorescence

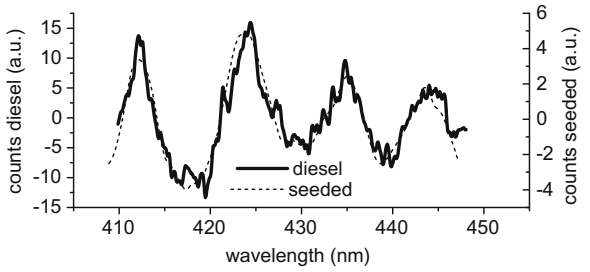

Fig. 4. Spectra after subtraction of the linear fit, see text for details. This example represents a good match between both spectra, for which $\alpha = 0.93$.

intensity $I \equiv I(p,T)$ is taken as the sum of all pixel values in a seeded spectrum, and the CH_2O spectral structure intensity $S \equiv S(p,T)$ (Fig. 4) is taken as the sum of the absolute pixel values of the CH_2O structure (see above). Their ratio $\gamma(p,T) \stackrel{\text{def}}{=} I/S$ is assumed to be independent of chemical environment, as explained above. By definition, $\gamma(p,T) \geqslant 1$. This I/S ratio γ is a measure for the contribution of the spectrally unstructured CH_2O fluorescence to the total CH_2O fluorescence intensity. It is assumed to be valid for engine spectra as well. In the range of interest for the present experiments (that is, 0.12–0.14 MPa nominal boost pressure; inlet air heating up to 40 °C; CA near TDC), no significant change in the I/S ratio was observed with pressure, and we found that $\gamma(p,T)$ could be parameterized, by a simple expression involving temperature only

$$\gamma(p,T) \equiv \gamma(T) = -5.22 + 0.011\,T + 3.7 \cdot 10^{-6} T^2 \quad (T \text{ in K}) \tag{1}$$

as shown in Fig. 6. Using this parameterisation, the total CH_2O fluorescence intensity in an engine spectrum, I_T can now be derived from the intensity of the spectral structure in an engine spectrum, S^e by

$$I_T = \begin{cases} \gamma(T)\alpha S^e & \text{if } \alpha \geqslant \alpha_{thr} \\ 0 & \text{if } \alpha < \alpha_{thr} \end{cases} \tag{2}$$

The spectral structure intensity from CH_2O (i.e. αS^e) will be denoted as $S^e_{CH_2O}$.

5. Method of quantification

A variety of phenomena has to be accounted for in transforming the CH_2O LIF signals into concentrations, i.e. the attenuation of the laser sheet and fluorescence trapping, the thermal population of

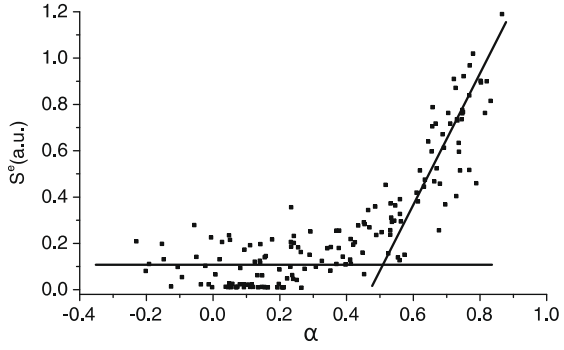

Fig. 5. Intensity of the spectral structure vs. α, for *n*-heptane as a fuel, SoD at 4.5° before TDC (bTDC). The threshold value for α has been determined from the intersection of the trend line through points in the region of high fit parameter values and the average spectral structure intensity for low fit parameter values. The fluorescence band of light (like shown in Fig. 3) has been binned into four parts, on a single shot basis, to obtain more data points without significantly sacrificing signal to noise ratio.

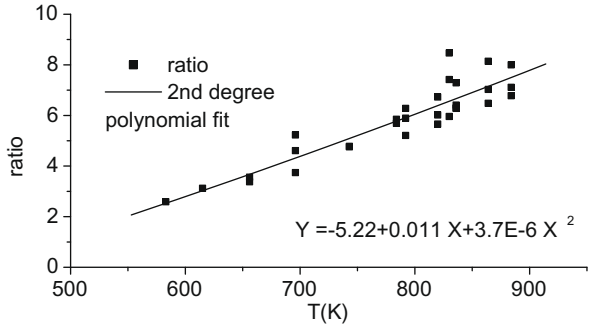

Fig. 6. Ratio $\gamma(T)$ of CH_2O total intensity and CH_2O spectral structure intensity vs. temperature.

the level probed, the loss of population in the excited state by quenching and internal conversion and the collection efficiency of the detection system [21]. The crank angle dependent fluorescence of the seeded CH_2O provides the pressure- and temperature-dependence of the LIF intensity (in air). By varying the boost pressure of the motored engine, the in-cylinder pressure can, to some extent, be varied independently. Two measurement series for the CH_2O LIF intensity vs. crank angle (CA) are shown in Fig. 7. The data basically show that the CH_2O fluorescence intensity is independent of pressure and temperature, implying that a change in the number density (by a volumetric change) is balanced by an altering LIF yield per molecule. We will assume that this also holds in the fired engine, so that the CH_2O LIF intensity is influenced only by differences in chemical environment (as compared to the seeding measurements) and by attenuation of the laser sheet and the fluorescence. This is justified by the fact that CH_2O is observed mainly before the onset of hot combustion, i.e. when the in-cylinder conditions still resemble those in a motored engine.

To assess the influence of the chemical environment, CH_2O was seeded into a fired engine. At crank angles when fuel vapour is already around, but just before CH_2O is formed by combustion, the intensity of CH_2O stucture shows a decrease of roughly 25% relative to a run without fuel injection. This is a combined effect of changes in quenching rate and optical transmission (around 90%, Fig. 8), indicating that the intensity might be influenced by a change in chemical environment, but not critically so. The change in quenching rate of around 15% relative to the motored engine is taken as the uncertainty in the quenching rate.

The laser sheet attenuation by spray 1 has been estimated by comparing the N_2 Raman intensity in between the two sprays (Fig. 1) in a motored cycle to that of a fired cycle. The assumption here is that, at a given boost pressure, the N_2 density is a function of crank angle only, whether or not fuel is injected. That is, the small density increase due to the injected fuel is neglected. Since the Raman scattering intensity is proportional to the incident laser intensity, irrespective of the chemical environment, it can be used for laser sheet attenuation measurements. The region where scattered light from the injector interferes with the Raman signal has been excluded from analysis. The transmission through spray 1 is depicted in Fig. 8 (start of delivery at 4.6° bTDC). The attenuation is seen to gradually increase with time after SoD (aSoD), plotted only for the range of interest for CH_2O. We have used the trend line depicted in Fig. 8 to correct for laser intensity variations with crank angle. The trend line indicates the total attenuation caused by spray 1 and sets an upper limit to the effective attenuation used to correct the spatially integrated CH_2O spectral structure intensity. Fluorescence trapping by soot and PAHs (large and/or ionised PAHs can absorb significantly between 408 and 448 nm [22]) is estimated to be much less significant than the laser sheet attenuation, as the path the fluorescence has to travel through the

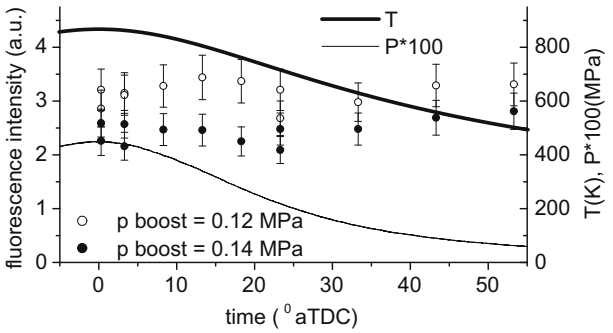

Fig. 7. Fluorescence intensity (formaldehyde is the only contributor) for seeded spectra at different crank angles, at nominal boost pressures of 0.12 MPa and 0.14 MPa, along with p and T for a nominal boost pressure of 0.12 MPa. Note that for an engine run, CH_2O is typically observed only a few CA around TDC.

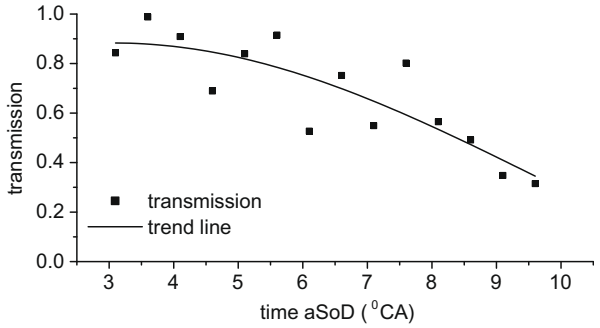

Fig. 8. Transmission of the laser sheet through spray 1 (n-heptane), derived from N_2 Raman scattering; SoD at 4.6° bTDC, probed through centre, 6.5 mm below the cylinder head.

attenuating spray is shorter than the absorption path of the laser sheet. Moreover, the highest soot concentrations occur downstream of the CH_2O region. Only late in the stroke, during the quasi-steady state combustion, when hardly any CH_2O is detected, PAH might partly overlap with CH_2O [8] and fluorescence trapping may be an issue. We decided to neglect fluorescence trapping. Window fouling along with laser intensity has been tracked by monitoring the N_2 Raman intensity regularly during a motored run.

To assess the temperature of the air that mixes with the cold fuel, in-cylinder air temperatures prior to combustion have been derived from in-cylinder pressure measurements (see Appendix A). For typical values of ϕ in the probe volume (between 2.0 and 3.5, see Section 6.2), adiabatic mixture calculations indicate that the relatively cold fuel induces a cooling of the air–fuel mixture of typically 200 K relative to the in-cylinder air. Once the combustion has started, the pressure is expected to be uniform throughout the cylinder, but the temperature may exhibit large spatial fluctuations. Simulations show, however, that by the time CH_2O is formed, not much heat has been released yet. A typical result for the homogeneous reactor is plotted in Fig. 9, suggesting that the local rise in temperature does not exceed about 300 K. As a combined effect of cooling due to the cold fuel and heating by chemistry, we assume the local temperature to rise only around 100 K above the global mean air temperature as extracted from the in-cylinder pressure curve. Only when CH_2O starts to be consumed rapidly during the rapid rise of the rate of heat release (RoHR), this estimate will probably be too conservative.

The local temperature is estimated to be uncertain by 100 K, which boils down to a 20% uncertainty in the measured concentration, caused by the strong dependence on temperature of the background contribution due to CH_2O. From the seeded measurements,

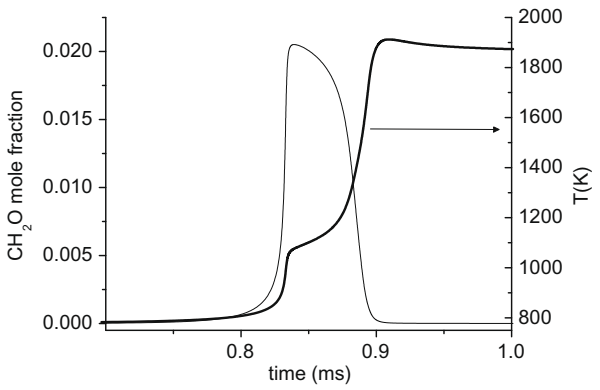

Fig. 9. Simulated CH_2O concentration vs. the time elapsed after the chemistry has been "switched on", along with the temperature for a homogeneous reactor of n-heptane and air. The equivalence ratio is 2.5, the initial temperature 780 K, and the pressure is 4.38 MPa.

it is concluded that the product of CH_2O concentration and laser intensity is uncertain by 12%, as estimated from fluctuations in the fluorescence intensity. The quenching rate is uncertain by 15%, as described above and the laser sheet transmission is uncertain by 10%. Taking these and some other (minor) uncertainties together, like the window fouling correction via the N_2 Raman signal and a slight uncertainty in absorption cross-section within the temperature error bar, we estimate the accuracy of the CH_2O concentration, up to the rapid rise of the RoHR, equal to 40%. After the onset of the hot combustion, the local uncertainty in temperature increases, resulting in an increase in the error to about 50%.

6. Results and discussion

6.1. Excitation of the 4_0^1 and $4_0^1 2_0^1$ bands, a comparison

Both the excitation of the 4_0^1 band and of the $4_0^1 2_0^1$ band were investigated. For the former, the readily available 3rd harmonic of the seeded Nd:YAG laser was used, for the latter the frequency doubled output of the dye laser. The tuning range of the dye laser allowed to scan off-resonance. The simulation program PGOPHER [13] indicated that, under typical engine conditions, the absorption cross-section of CH_2O would be about 3.5 times higher at the maximum of the $4_0^1 2_0^1$ band than for the wavelength range in the 4_0^1 band.[1] This would facilitate a higher ratio of formaldehyde to non-formaldehyde fluorescence, providing a route for 2D fluorescence images that are easier to interpret.

The seeding measurements provide well-defined conditions to study the excitation efficiency ratio. This quantity is defined here as the fluorescence yield upon excitation with the dye laser, divided by the fluorescence yield upon excitation with the 3rd harmonic, both normalised by the respective laser intensities. 2D data were integrated over the field of view. The result as a function of crank angle (i.e. temperature and pressure) is given in Fig. 10. The increasing efficiency ratio with crank angle is ascribed to a different dependence of the absorption cross-section on p and T for both vibrational bands, as is predicted by PGOPHER. At engine conditions near TDC, the ratio is 1.1 ± 0.4, in contrast to the predicted factor of 3.5 mentioned above. In the fired engine, an efficiency ratio of 1.5 ± 0.3 was obtained. The reason behind this discrepancy between experiment and prediction by PGOPHER is still unclear.

To investigate what part of the dye-laser-excited fluorescence originates from CH_2O, formaldehyde was excited both on- and

[1] The oscillator strength for the 4_0^1 band was not listed. It was derived from the absorption spectra reported by Co et al. [23].

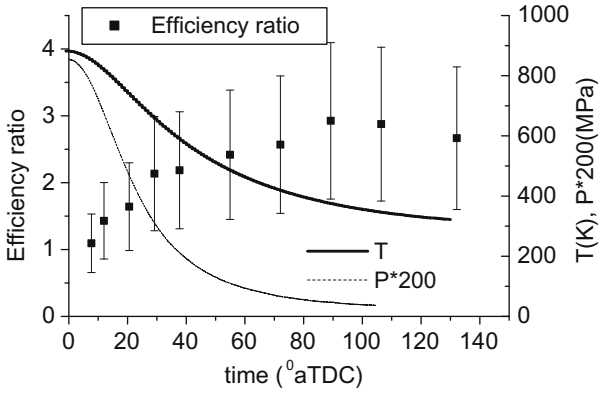

Fig. 10. Excitation efficiency ratio as a function of CA. The pressure and temperature as a function of CA are portrayed as well.

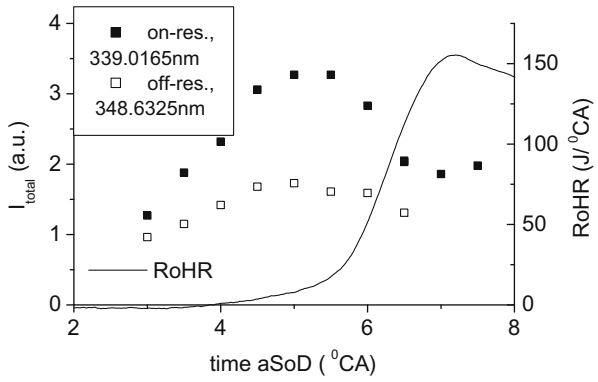

Fig. 11. Total fluorescence for on- and off-resonance, and the rate of heat release (solid line) as derived from the in-cylinder pressure curve.

off-resonance. For on-resonance, a wavelength close to the maximum absorption cross-section (339.017 nm), as calculated by PGOPHER, was chosen. The off-resonance wavelength was 348.6 nm, chosen to make sure not to excite formaldehyde via the adjacent 4_0^1 and 4_0^3 bands.[2] The total integrated fluorescence I_{total} for the on- and off-resonance wavelength, using the spectrograph, is depicted in Fig. 11. Both fluorescence signals show a similar behaviour as a function of crank angle, which indicates that the off-resonance fluorescence is also related to cold flame phenomena, like the on-resonance CH_2O fluorescence. Both peak around 5° aSoD, but the off-resonance fluorescence intensity only reaches about 55% of the on-resonance fluorescence intensity.

The same ratio between on- and off-resonance fluorescence was observed when 2D images were taken, using optical filters rather than a spectrograph. This is in line with the expectation, as the SPF450 filter used transmits in the same wavelength range as the range used with the spectrograph. Excitation of other cold flame species is also suggested by 2D images, as on- and off-resonance images generally have the same spatial structure.

The difference between on- and off-resonance fluorescence intensity is not necessarily ascribed completely to CH_2O, as many cold flame species absorb stronger towards the UV, e.g. aldehydes and ketones [24,25]. This is corroborated by the method derived in Section 4 to extract the total CH_2O fluorescence from the CH_2O spectral structure intensity. Applying this method, the CH_2O spectral structure intensity (not given in Fig.11) at the time of the maximum in on-resonance signal was multiplied by 8.6 (using Eq. (2) for $T = 950$ K) to get the total CH_2O fluorescence. At this time, however, the difference between the on- and off-resonance fluorescence is larger, i.e. roughly 18 times $S^e_{CH_2O}$, indicating that indeed the difference between on- and off-resonance cannot be ascribed completely to fluorescence from CH_2O.

Because of its robustness, higher output power and the slightly lower relative non-formaldehyde background, the 3rd harmonic of the Nd:YAG laser was employed for the CH_2O measurements during combustion.

6.2. CH_2O concentration and comparison to numerical data

Fig. 12a and b shows the experimental CH_2O concentration for *n*-heptane as a fuel, obtained by excitation at 355 nm, and the simulated concentrations for homogeneous reactors in a range of initial conditions (see caption), respectively. The simulations depicted have been performed with the LLNL PRF mechanism, yielding CH_2O concentrations of roughly 15% higher than the concentrations given by the Peters mechanism, for equivalence ratios between 2.0 and 3.5. This is the range of equivalence ratios in the FOV for the present diesel spray, as has been derived from the Schlieren measurements in the Eindhoven high-pressure high-temperature cell (EHPC) [26], using the model of Naber and Siebers [27]. The experimental concentration is about a factor of five lower than the concentration calculated for the LLNL PRF mechanism. The simulated concentration should be regarded as an upper limit, however, as in the engine not all fuel ignites simultaneously. This has also been suggested by Hildingsson et al. [28] who showed that naturally occuring formaldehyde might serve as a fuel tracer. Note also that the experimental concentration is an average over the FOV. In the centre of the FOV, the concentration is consistently 1.5–2 times as high as the average, as can (qualitatively) be seen in Fig. 13a. The reason behind these differences in concentration in the radial direction will be addressed in Section 6.5. Considering the error bars, the concentration in the centre of the FOV is in reasonable agreement with the simulated concentration.

For experiments with diesel in spray 2, the CH_2O spectral structure intensity is comparable to that for *n*-heptane as a fuel and as such, the concentrations are comparable as well.

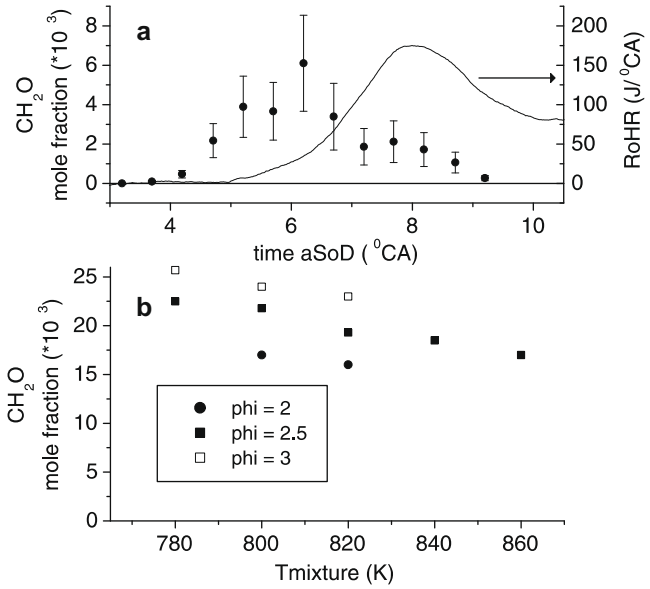

Fig. 12. (a) Experimental CH_2O concentration for *n*-heptane as a fuel vs. °CA, along with the RoHR. (b) Simulated CH_2O concentration using the LLNL PRF mechanism, for $p = 4.38$ MPa and a range of initial mixture temperatures.

[2] A scan in a Bunsen burner (atmospheric pressure) showed no formaldehyde spectral stucture in the fluorescence emission spectrum at this wavelength.

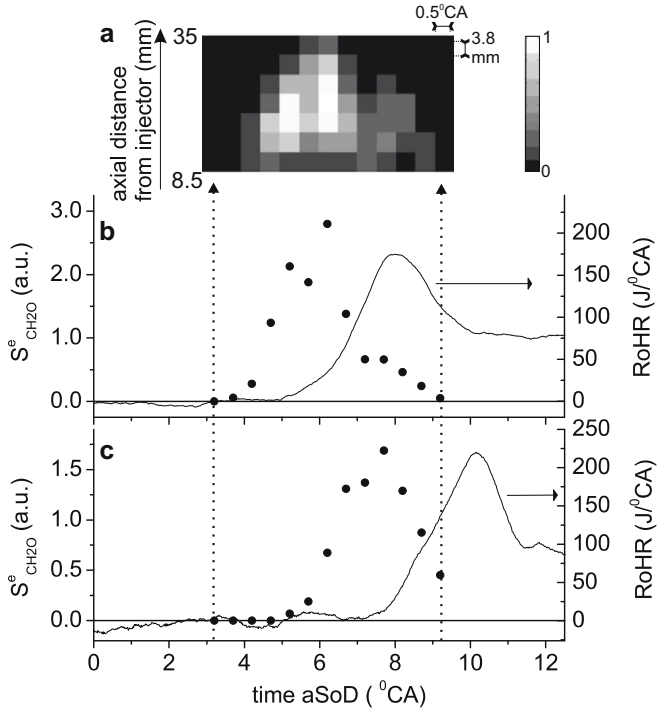

Fig. 13. (a) $S^e_{CH_2O}$ from the centre of spray 1 as function of time aSoD (same scaling as in (c)) and distance from injector. The grayscale is linear in intensity, black and white mean no signal and maximum signal, respectively, as indicated by the colorbar. The FOV ends at 36.5 mm. *n*-Heptane was used as a fuel, SoD was 4.6° bTDC. The probe height was 6.5 mm below the cylinder head and the sheet was only 2 mm wide. (b) $S^e_{CH_2O}$ from (a) space integrated vs. time aSoD. (c) As in (b), but SoD at 14.6° bTDC.

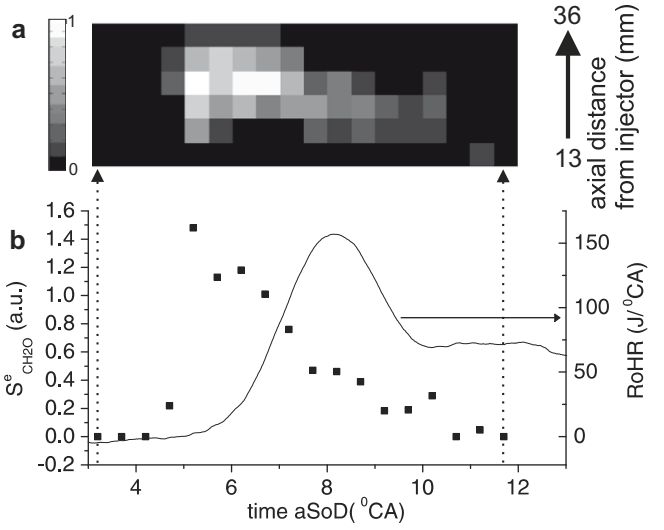

Fig. 14. CH_2O spectral structure intensity for SoD at 4.5° bTDC, spray 2, *n*-heptane as a fuel. The laser sheet was 8 mm wide and 0.5 mm thick, traversing the cylinder 5 mm below the cylinder head. (a) Time and space resolved intensity of the CH_2O spectral structure. The abscissa gives the time aSoD, the ordinate the distance from the injector. (b) Intensity of the CH_2O spectral structure in (a) spatially integrated.

6.3. Temporal information for different injection timings

A typical fluorescence band of light is depicted in Fig. 3c. The spray was probed close to the spray axis, with a laser sheet of about 2 mm in width, traversing the cylinder 6.5 mm below the cylinder head. Thus, the laser sheet intersects the spray 4.6 mm below the injector. A small sheet width was chosen in order to achieve some degree of spatial resolution. The CH_2O structure on top of a background can be seen as the four brighter vertical bands of light in Fig. 3c. The area where the band of light was present below the injector (Fig. 3c) was subdivided in typically seven spatial parts of five strips (strip: row of pixels) and these separate parts (integration over five strips) were analysed individually. For these seven parts, the temporally resolved intensity of the CH_2O spectral structure (extracted via the method described in Section 4) is depicted in Fig. 13a.[3] The brightness of a single square indicates the intensity of the CH_2O spectral structure for one of these spatial parts for a certain time aSoD. The brightness of each square is linear with the value of $S^e_{CH_2O}$, where black and white mean no signal and maximum signal, respectively. The spatial parts are displayed along the ordinate. The CH_2O spectral structure intensity from Fig. 13a was integrated over the seven parts of five strips. The result from integration is plotted in Fig. 13b vs. time aSoD. The figure shows clearly that the CH_2O is formed before the start of the main heat release, it peaks around the start of the rapid rise of heat release and decreases fastly once more heat is released, corroborating the result of Kosaka et al. [7] and Lachaux and Musculus [18]. The timing of CH_2O appearance shifts along with the heat release, as illustrated by the two injection timings shown. The CH_2O spectral structure intensity from spray 2 is plotted in Fig. 14. The laser sheet traversed the cylinder at 5 mm below the cylinder head, had a width of 7 mm and was 0.2 mm thick. Even though the CH_2O structure remains longer visible than for spray 1 (most probably because of the strong attenuation experienced in spray 1, later in the stroke), it still almost disappears before the end of the injection. Occasionally, a little bit of CH_2O is detected during the diffusion burn, close to the injector where the hot combustion has not yet started.

For diesel, the intensity of the CH_2O spectral structure as a function of time is shown in Fig. 15 and the result is similar to the result for *n*-heptane. Again, formaldehyde shows up before the main heat release and is consumed rapidly when the combustion temperature rises. The spectral measurements allow to identify formaldehyde even when the soot luminosity starts to rise. For spray 2, CH_2O is again detected until later in the stroke. The difference between both sprays is larger than for *n*-heptane, in line with expectation since diesel gives rise to significantly more attenuation.

Note that for exceptionally late injection, starting at 3.5° aTDC, the formaldehyde fluorescence does not go down to zero later in the stroke, as illustrated by Fig. 16 for *n*-heptane, spray 2. This indicates that the combustion never advances fully into its second hot stage, in accordance with results reported in Ref. [18] for a large ignition delay. From the indicated mean effective pressure (IMEP) it can also be inferred that the combustion is incomplete. The IMEP

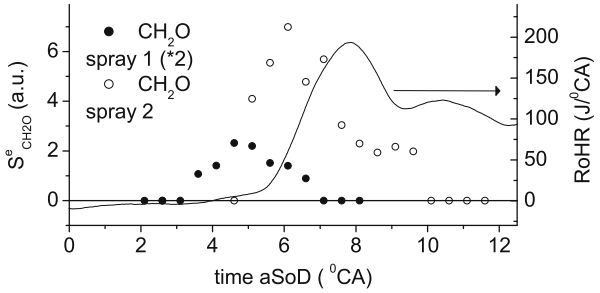

Fig. 15. $S^e_{CH_2O}$ for diesel, SoD at 4.5° bTDC. The laser sheet was 7 mm wide, probing the fuel spray 7.5 mm below the cylinder head.

[3] Here, 'axial distance' refers to the distance from the injector, parallel to the cylinder head. Since the spray angles down under 10^0 with the cylinder head, the distance in the axial direction of the spray is 1.5% larger.

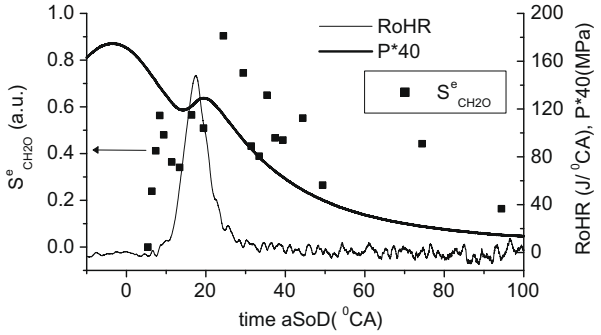

Fig. 16. $S^e_{CH_2O}$ for SoD at 3.5° aTDC, 15° injection duration, *n*-heptane as fuel, spray 2. The laser sheet was 7 mm wide, probing the fuel spray 3.5 mm below the cylinder head.

is 306 kPa for this injection timing, while for an equally long injection duration starting at 4.5° bTDC, the IMEP is 353 kPa.

6.4. Relation between CH_2O fluorescence and total fluorescence

6.4.1. In a spray

Detection of light from a spray in the formaldehyde emission wavelength range does not necessarily imply occurrence of CH_2O. To make this statement more quantitative, Fig. 17a displays the total amount of light (P) detected vs. the fit parameter α (see Section 4). Timings later in the stroke have been excluded in order to refrain from taking into account significant contributions from PAH and soot. Beyond the threshold value for the fit parameter (to the right of the dotted line $\alpha_{thr} = 0.5$), part of the light is ascribed to CH_2O. Below α_{thr}, still light intensities of 25% of the maximum occur, while none of it is likely to originate from CH_2O. Note that the graph serves only as a typical example. The number of occurrences below α_{thr} depends, amongst others, on the measurement position in the spray. It can be concluded that one has to be careful in ascribing fluorescence to formaldehyde, even at timings around the maximum of CH_2O fluorescence.

Fig. 17b displays the average ratio of the total CH_2O intensity (I_T, structure and background due to formaldehyde) and the total amount of light, vs. time aSoD, using the same data. Only data points for which it was decided that CH_2O was present (i.e. $\alpha > \alpha_{thr}$) were taken into account. The ratio does not critically depend on measurement timing. This rather constant ratio suggests that the background signal is related to CH_2O and originates from other species formed during the cold combustion, like other aldehydes and ketones (that might be around in significant quantities), as has also been suggested by Amnéus et al. [5]. Literature was checked on spectroscopy of aldehydes and ketones to see how these species might fluoresce in the present detection wavelength range. Unfortunately, only data on the absorption spectra below typical cold flame temperatures were found. The absorption and emission spectra of aldehydes and some ketones (symmetrical methyl-substituted acetones) have been recorded by Hansen and Lee [24,25]. They show that these species fluoresce in the same wavelength range as CH_2O but hardly absorb at 355 nm at room temperature. Kosaka et al. [7] excited acetaldehyde and ketone at 355 nm in a test vessel (0.1 MPa, 353 K). No fluorescence between 390 and 420 nm was detected. Innes and Giddings [29] suggest that for acetaldehyde, hot bands only play a minor role at 523 K. At 950 K (typical cool flame temperature), the absorption spectrum could well be slightly red-shifted as compared to lower temperatures, but it is hard to estimate to what extent this might contribute to emission.

The dye laser experiments shown earlier suggest that at 348.5 nm (off-resonance for formaldehyde), cool flame species are

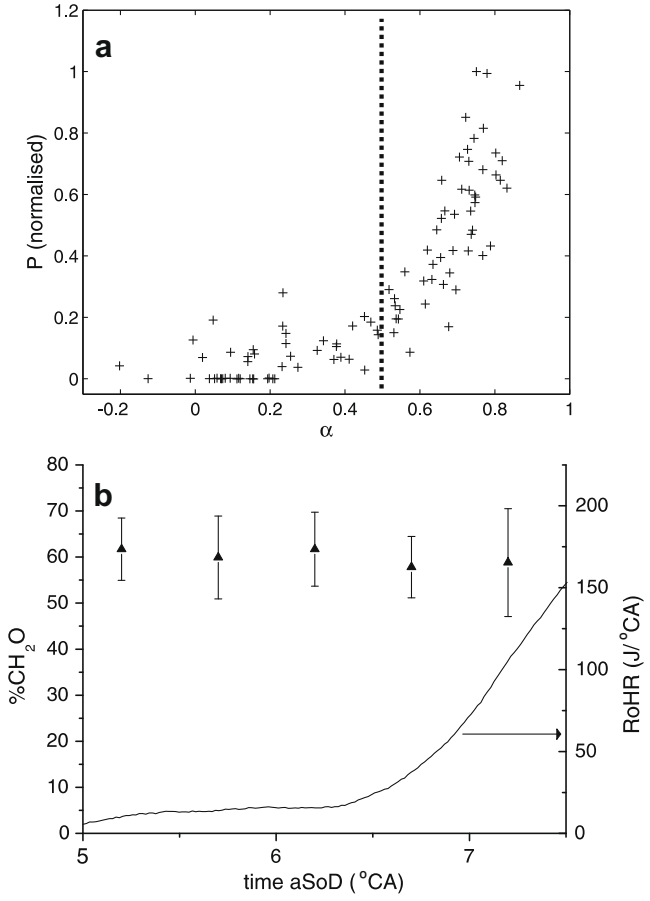

Fig. 17. (a) The total amount of light P detected vs α. The fluorescence band was again binned into four parts, on a single shot basis, as for Fig. 5. The abscissa denotes the value of the fit parameter α, the vertical dotted line its threshold value. (b) Percentage of CH_2O ($=100 * I_T/P$) vs. time aSoD, along with the RoHR.

excited. Thus, they might contribute – although with lower intensity – to the fluorescence at 355 nm excitation as well.

To conclude this part, we think the non-formaldehyde background originates for a significant part from cool flame species and that interpreting the fluorescence as indicative for the cool flame is a sensible approach. In the spray, however, fluorescence upon 355 nm excitation cannot be interpreted unequivocally as indicative for CH_2O.

6.4.2. PCCI/HCCI conditions

Premixed charge compression ignition conditions were obtained by injecting only between 24.5° and 16.0° bTDC. The cold flame started well after the end of the injection at around 14.0° aSoD. In this situation, the probability of detecting significant fluorescence in the case of α being below its threshold, was clearly smaller than under spray conditions. Even when the CH_2O fluorescence signal decreased (interpreted as consumption of CH_2O), this probability remained low. These data suggest that in PCCI (and HCCI) measurements, interpreting the fluorescence as originating from CH_2O is probably justified.

6.5. Spatial information

Fig. 13a shows that CH_2O in spray 1 first appears near the injector, then expands its range further downstream, and finally disappears, with its range retracting towards the injector. We believe the extension of CH_2O in more and more downstream direction is mainly CH_2O travelling down the jet rather than local formation as the distance from the injector is correlated to the time after

injection. The speed at which the CH_2O signal propagates radially outward corresponds to the fuel vapour speed of 5.0 ± 0.5 mm/°CA. The vapour speed was determined from Schlieren measurements in the EHPC using the same injector type, fuel injection pressure and ambient conditions as in the engine experiments. Formaldehyde retreating towards the injector has also been observed by Lachaux and Musculus [18] for low-temperature combustion. We ascribe it to consumption during the hot combustion stage because the retreat coincides with the fast rise in the rate of heat release. Seperate high-speed images show that the hot diffusion flame approaches the injector as indicated by the upstream propagation of luminous soot (see supplementary material in Ref. [11]). For the SoD = 4.6° bTDC case, the increase in temperature closer to the injector is corroborated by OH LIF measurements (not shown here), indicating that OH typically emerges at 8° aSoD and that it gets as close to the injector as CH_2O within 1 °CA later.

The results can be cast into the following schematic picture (Fig. 18) for the "life-cycle" of CH_2O: in going from the injector to the spray-tip, one essentially follows the time-axis of a package of fuel, somewhat complicated by the still developing flame. The cold fuel in the package entrains hot in-cylinder air, evaporates, and after a while it ignites and CH_2O is formed. Finally, hot combustion sets in and formaldehyde is consumed. Due to inhomogeneity in the spray, fuel ignites over quite a time span for different packages. For formaldehyde, this means that its formation occurs in a range of distances from the injector, as depicted in Fig. 18. Because of the developing flame, temperatures and pressures continue to rise, and new fuel packages advance earlier into the hot combustion stage, resulting in CH_2O retreating towards the injector.

A time sequence of 2D images in Fig. 19 shows the consumption of CH_2O towards the injector, in the centre of the spray. Spectral data (recorded seperately from the 2D images) are of help in interpreting these 2D data. The higher intensity closer to the injector is most likely caused by scattering from the liquid spray. The signal first grows stronger in time and progresses downstream. Then, CH_2O retreats towards the injector, coinciding with the start of the rapid rise of the RoHR. Spectral data from the area indicated by the grey rectangle at 7.8° aSoD suggest that the fluorescence here is not likely to originate from CH_2O. Its presence cannot be ruled out, however, as in some strokes, some CH_2O structure was seen downstream. The strong fluorescence in the regions of the grey dotted rectangles at 8.3° and 8.8° aSoD originates from (precursors of) soot. Note that the width of the slot did not allow to image the outer part of the spray (in swirl direction).

The literature seems to contain conflicting results as to whether or not formaldehyde disappears completely later in the combustion stroke. In [8] (21% O_2, moderate soot condition), Idicheria and Pickett conclude that CH_2O persists during the quasi-steady state. Although they have good reasons for this conclusion, based on simulations and on results obtained by varying the amount of soot formed, they provide no evidence by performing spectral measurements. They remark that persistent formaldehyde during the quasi-steady state combustion might also be suggested by measurements reported by Bruneaux et al. [30], based on a weak LIF signal upstream of OH. Kosaka et al. [7], however, showed that the spectral signature of formaldehyde disappears after the start of hot combustion, even relatively close to the injector, where the concentrations of soot and PAH were shown to be small. In the present work, the CH_2O structure disappears completely.

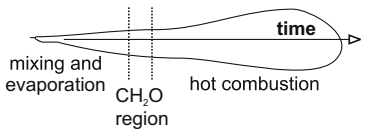

Fig. 18. Schematic picture of a steady-state flame. The width of the CH_2O region depends on the actual stage of the flame development.

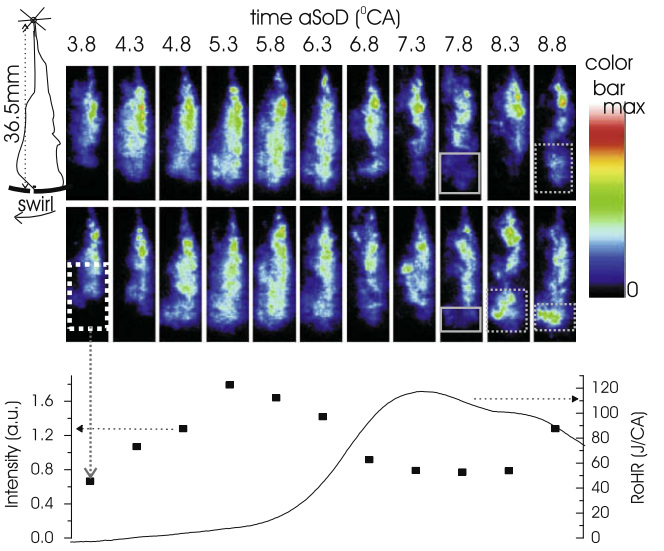

Fig. 19. Upper part: 2D images for 355 nm excitation, *n*-heptane as a fuel, SoD at 4.6° bTDC and 15° injection duration. The laser sheet was 7 mm wide, the probe height 5 mm below the cylinder head. The numbers above the snapshots denote the time aSoD (°CA). Two characteristic snapshots for each timing are given. All snapshots have the same intensity scale. At the left side, a schematic view of the spray is shown. The meaning of the rectangles overlaid on the snapshots is given in the text. The rate of heat release and integrated intensity, averaged over five laser shots is depicted in the lower part. The area of integration is given by the white dotted rectangle in the lower left snapshot, taken such to exclude fluorescence from the liquid spray.

7. Conclusions

Formaldehyde has been detected as a function of place and time in a fuel spray in an optically-accessible diesel engine, for a variety of injection timings, using a novel technique to extract the CH_2O contribution from fluorescence spectra. The method shows that a considerable part of the structureless background can be due to non-formaldehyde fluorescence. Both the 3rd harmonic of the Nd:YAG laser (355 nm, excitation of the 4_0^1 band) and a frequency-doubled dye laser (339 nm, excitation of the $4_0^1 2_0^1$ band) have been applied. The excitation efficiency was found to be comparable for both sources, in contrast to the computed result. The Nd:YAG laser was preferred because of its higher power, robustness, and the lower relative non-formaldehyde background. Formaldehyde shows up typically 2 °CA before the rapid rise of RoHR, relatively close to the injector and is transported downstream. Once the RoHR rises, CH_2O retreats towards the injector, disappearing almost completely during the mixing-controlled combustion.

For quantification, the dependence of the LIF intensity on pressure and temperature was accounted for by using the CA-dependent LIF intensity of seeded CH_2O spectra from a motored engine. The laser sheet attenuation was monitored using the N_2 Raman intensity after traversing the spray. The quenching was shown not to be critically dependent on the chemical environment by seeding CH_2O into a fired engine. Data were fully calibrated by seeding a known CH_2O concentration into a motored engine. The most critical parameter in extracting the CH_2O concentration from the fluorescence spectra is the local temperature, affecting the CH_2O contribution relative to the background. The experimental CH_2O maximum local mole fraction for *n*-heptane (0.012 ± 0.004) is in reasonable agreement with the simulated concentration in a

homogeneous reactor of *n*-heptane and air. Diesel and *n*-heptane give similar concentrations.

Acknowledgments

The authors would like to acknowledge Leander Gerritsen and Peter Claus for their technical assistance. Dennis van Erp is acknowledged for performing the Schlieren measurements. The research is financially supported by Technology Foundation STW.

Appendix A. Calculation of temperature

Because the temperature of the in-cylinder air entrained by the sprays is of importance for the quantification, the method of calculating the temperature in the motored engine is presented here. To determine in-cylinder temperatures accurately, the temperature dependent specific heat constants, the heat transfer to the cylinder wall and blowby have to be accounted for. In taking into account these factors, the temperature is regarded to be homogeneous throughout the cylinder, i.e. the mass averaged bulk temperature is calculated. The effect of boundary layers is addressed at the end.

The theoretical pressure curve was determined by a custom made code, taking into account the change in internal energy via

$$dU = dQ - p \cdot dV + h \cdot dm \tag{3}$$

where dU is the change in internal energy, dQ the heat flux, p the pressure, dV the volume change, h the enthalpy per unit mass and dm is the mass loss via blowby. To calculate the change in pressure and temperature, the temperature dependent specific heat constants from the Chemkin Thermodynamic database [31] have been used. The ideal-gas law was applied as an equation of state.[4]

In addressing the heat transfer to the cylinder walls, only the convective heat transfer Q_{conv} is taken into account, as this is the dominant source of heat transfer. It is governed by

$$\frac{dQ_{conv}}{dt} = -h_{conv} \cdot A(T - T_w) \tag{4}$$

where A is the (crank angle dependent) area of the cylinder wall, T denotes the in-cylinder temperature, T_w the wall temperature and h_{conv} is given by

$$h_{conv} = C_{conv} B^{m-1} p^m w^m T^{0.75-1.62\ m} \tag{5}$$

with C_{conv} the constant of heat conduction, B the bore, p the pressure and w the average speed of the gas [33]. The constant m is taken to be 0.8, a common value in the Woschni expression [34]. If the small swirl in the engine is neglected, w is given by

$$w = C_1 S_p \tag{6}$$

where $C_1 = 6.18$ during the inlet stroke and 2.18 during the compression. S_p is the average piston speed.

For the mass loss via blowby, Bernouilli's equation has been used (Appendix C of [12]). Therefore, the effective ring clearance (Rc) should be known. It was not, however. Moreover, the effective boost pressure was somewhat lower than the pressure set, mainly due to a filter in the inlet air channel, causing a lower air flow. These two unknowns served as fitting parameters in matching the theoretical pressure curve to the experimental pressure curve. The third fitting parameter was the constant of heat conduction C_{conv}. A variation around the experimentally determined value of 0.5 MW/m^2, as reported in [34], was employed. A typical fitting result is portrayed by Fig. 20. At the time of the inlet valve closing, the theoretical curve is fixed to the effective boost pressure. With the values of the fit parameters, the heat flux around TDC is 0.33 MW/m^2. The values of the fitting parameters are displayed in the figure. The fitted ring clearance and constant of heat conduction proved to be hardly dependent on experimental conditions (i.e. the boost pressure and inlet temperature), adding validity to the method. The temperature at TDC in the motored engine is 840 ± 15 K, instead of 867 K if heat transfer and blowby were not an issue.

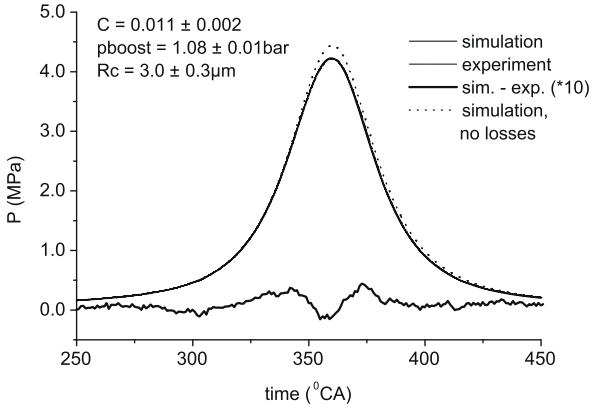

Fig. 20. The simulated and experimental pressure curve, along with the difference (multiplied by 10) of both. The simulated pressure for a nominal boost pressure of 0.12 MPa (effective boost pressure of 0.108 MPa) when no heat- and mass losses are taken into account is plotted as well. The inlet temperature was 40 °C. The fit parameters are listed. The experimental pressure is hardly visible due to the good overlap of experimental and simulated pressure trace.

Ferguson et al. [35] show that the temperature in the centre of an internal combustion engine is typically a few percent higher than the mass averaged bulk temperature. This difference should be appreciated. Their approach cannot be followed however, as we do not know the thickness of the boundary layer. An upper limit for the temperature in the centre can be obtained by setting the heat loss via convection to zero in the calculation described above (i.e. the only loss in internal energy is due to blowby). This way, a temperature of 864 K was found. We chose to set the temperature of the in-cylinder air in the centre to 855 ± 20 K.

[4] The effect of applying the Van der Waals law rather than the ideal-gas law as an equation of state has been investigated. The constants and approach of Zevenhoven [32] have been applied, yielding a TDC temperature lowered by less than 1%. This left us to conclude that under the pressures and temperatures experienced, the calculated temperature does not critically depend on the choice of the equation of state.

References

[1] Annual Energy Outlook 2009. <http://www.eia.doe.gov/oiaf/aeo>.
[2] R. van Basshuysen, F. Schäfer, Internal Combustion Engine Handbook, SAE International, Warrandale, PA, 2002. p. 439.
[3] T. Kim, J.B. Ghandhi, Proc. Combust. Inst. 30 (2005) 2675–2682.
[4] M. Richter, R. Collin, J. Nygren, M. Aldén, L. Hildingson, B. Johansson, JSME Int. J. 48 (2005) 701–707.
[5] P. Amnéus, M. Tunér, F. Mauss, R. Collin, J. Nygren, M. Richter, M. Aldén, M. Kraft, A. Bhave, L. Hildingsson, B. Johansson, SAE Paper 2007-01-0049, 2007.
[6] J.T. Kashdan, J. Papagni, SAE Paper 2005-01-3739, 2005.
[7] H. Kosaka, T. Aizawa, T. Kamimoto, Int. J. Eng. Res. 6 (2005) 21–42.
[8] C.A. Idicheria, L.M. Pickett, SAE Paper 2006-01-3434, 2006.
[9] L. Genzale, R.D. Reitz, M.P.B. Musculus, SAE Paper 2008-01-1330, 2008.
[10] R. Schießl, P. Pixner, A. Dreizler, U. Maas, Combust. Sci. Technol. 149 (1999) 339–360.
[11] R.J.H. Klein-Douwel, A.J. Donkerbroek, A.P. van Vliet, M.D. Boot, L.M.T. Somers, R.S.G. Baert, N.J. Dam, J.J. ter Meulen, Proc. Combust. Inst. 32 (2009) 2817–2825.
[12] J.B. Heywood, Internal Combustion Engine Fundamentals, McGrawHill, Singapore, 1989.
[13] C.M. Western, PGOPHER, a Program for Simulating Rotational Structure, 2007. <http://pgopher.chm.bris.ac.uk>.
[14] C.A. Smith, F.D. Pope, B. Cronin, C.B. Parkes, A.J. Err-Owing, J. Phys. Chem. A 110 (2006) 11645–11653.
[15] L.M.T. Somers, A.V. Evlampiev, L.P.H. de Goey, in: G. Skevis (Ed.), Proceedings of the 3rd European Combustion Meeting, ECM2007, Chania, Greece, 2007, Paper 22-14.
[16] H.J. Curran, P. Gaffuri, W.J. Pitz, C.K. Westbrook, Combust. Flame 129 (2002) 253–280.

[17] N. Peters, G. Paczko, R. Seiser, K. Seshadri, Combust. Flame 128 (2002) 38–59.
[18] T. Lachaux, M.P.B. Musculus, Proc. Combust. Inst. 31 (2007) 2921–2929.
[19] J.C. Weisshaar, D.J. Bamford, E. Specht, C.B. Moore, J. Chem. Phys. 74 (1981) 226–234.
[20] K. Shibuya, E.K.C. Lee, J. Chem. Phys. 69 (1978) 758–766.
[21] M.G. Allen, K.R. McManus, D.M. Sonnenfroh, P.H. Paul, Appl. Opt. 34 (1995) 6287–6300.
[22] A. Li, B.T. Drane, Astrophys. J. 572 (2002) 232–237.
[23] D.T. Co, T.F. Hanisco, J.G. Anderson, J. Phys. Chem. A 109 (2005) 10675–10682.
[24] D.A. Hansen, E.K.C. Lee, J. Chem. Phys. 63 (1975) 3272–3277.
[25] D.A. Hansen, E.K.C. Lee, J. Chem. Phys. 62 (1975) 183–189.
[26] R.S.G. Baert, P.J.M. Frijters, L.M.T. Somers, C.C.M. Luijten, W. de Boer, SAE Paper 2009-01-0649, 2009.
[27] J.D. Naber, D.L. Siebers, SAE Paper 960034, 1996, pp. 59–88.
[28] L. Hildingsson, B. Johansson, A. Hultqvist, G. Särner, M. Richter, M. Aldén, SAE Paper 2005-24-008, 2005.
[29] K.K. Innes, L.E. Giddings, J. Mol. Spectrosc. 7 (1961) 435–438.
[30] G. Bruneaux M. Augé C. Lemenand Comodia 2004, Japan, 2004, pp. 551–560.
[31] R.J. Kee, F.M. Rupley, J.A. Miller, Report No. SAND87-8215, Sandia National Laboratories, 1987.
[32] R. Zevenhoven, in: Proceedings of the First Biannual Meeting and General Section Meeting of the Scandinavian-Nordic Section of the Combustion Institute, Gothenburg, Sweden, 2001, pp. 103–108.
[33] G. Woschni, SAE Paper 670931, 1967.
[34] J. Chang, O. Güralp, Z. Filipi, D. Assanis, T. Kuo, P. Najt, R. Rask, SAE Paper 2004-01-2996, 2004.
[35] C.R. Ferguson, R.M. Green, R.P. Lucht, Combust. Sci. Techol. 55 (1987) 63–81.
[36] R.A.L. Tolboom, N.J. Dam, N.M. Sijtsema, J.J. ter Meulen, Opt. Lett. 28 (2003) 2046–2048.